Applied Physics A (2021) 127:618
https://doi.org/10.1007/s00339-021-04784-3

Applied Physics A
Materials Science & Processing

Significance of surface roughness in the supercapacitor activity of nickel-based electrodes

Muharrem Kunduraci[1] · Doğan Çirmi[2] · Selda Doğan Çalhan[3] · Uğur Çağlayan[4]

Received: 11 June 2021 / Accepted: 19 July 2021 / Published online: 23 July 2021

Abstract

Nickel-based thin film electrodes were electrodeposited onto copper substrate using a deep eutectic solvent. The supercapacitor performance of these electrodes in alkaline KOH solution was greatly enhanced by altering surface roughness of coatings. In order to create a rougher surface, two paths were followed. In the first path, Ni-only coatings were prepared at different deposition potentials and smooth-to-rough transition in surface morphology took place at higher potentials due to increasing emission of hydrogen bubbles. In the second path, Ni–Zn binary coatings with varying zinc concentration were electrodeposited and surface roughness was formed by dealloying zinc element from the electrodes as corroborated by Scanning Electron Microscopy and Atomic Force Microscopy results. In both paths, noticeable improvements in the capacitance of nickel electrodes were observed upon the apperance of rougher surface. A linear relationship was discovered between cathodic peak currents and polarization values in the cyclic voltammetry scans of electrodes, possibly for the first time here in literature. The increase in polarization was explained by the decrease in electrode conductivity proved by dwindling of metallic nickel peaks in X-ray diffraction upon electrochemical testing.

Graphic Abstract

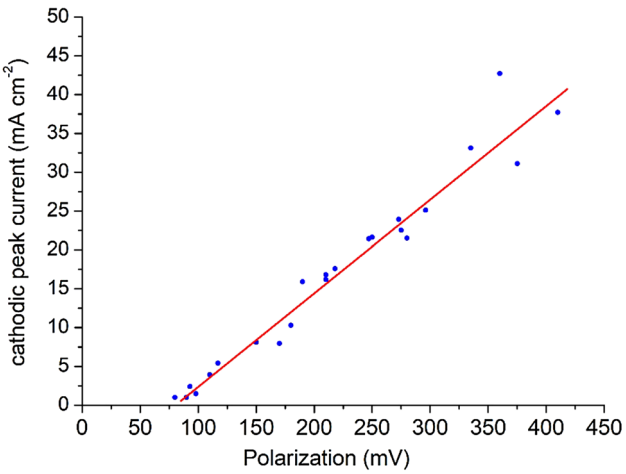

Keywords Supercapacitor · DES · Nickel · Thin film

1 Introduction

Batteries and supercapacitors are the most popular electrochemical energy storage systems and critical for many sectors including transportation, stationary storage and consumer electronics. While batteries offer much higher energy

✉ Muharrem Kunduraci
kunduraci.m@hotmail.com

Extended author information available on the last page of the article

densities, supercapacitors stand out in applications where high power density is required. Among the supercapacitor materials, nickel-based materials have gained much interest in recent years due to their relatively low cost, easy synthesis and high specific capacitance [1–3]. In order to reach high specific capacitance, supercapacitor material needs to have high electrical conductivity as well as high surface area. Various morphologies with high surface areas including nanowires, nanoparticles and thin films have been reported previously [4, 5]. Different techniques such as hydrothermal, electrodeposition and sol–gel were utilized in the synthesis of these materials [6–8]. While nanostructuring of electroactive material yields good capacitance and rate performance, they suffer from low volumetric energy density. On the other hand, thin films are easier to manufacture and do not contain electrochemically inactive components such as carbon and binder.

In this study, we electrodeposited Ni-only and Ni-Zn binary coatings onto copper substrate and studied the interplay between morphology and capacitive behavior of electrodes. Specifically, an attempt was made to boost the electrochemical activity of nickel electrodes by surface roughening of thin films. To our best knowledge, such a study has not been reported so far with nickel-based materials. Two totally different paths were taken to achieve such a goal. In Ni-only films, a wide range of deposition potentials was chosen and its effect on the surface morphology of films was investigated. In Ni-Zn coatings, films with varying zinc concentration were initially prepared and it was followed by anodic dealloying of zinc from films. The dealloying process was found to alter smooth film surface into a rough one, thereby siginificantly affecting capacitive behavior in return.

Ethaline deep eutectic solvent (DES) having a molar ratio of 1:2 choline chloride-ethylene glycol was chosen for the electrodeposition of thin films in our study. DES was first noted by Abbot et al. [9]. DES can be considered as a new generation ionic liquid, generally consisting of an organic salt and at least one hydrogen bond donor, and having a melting point lower than any of its individual components [10]. The popularity of deep eutectic solvents has increased significantly in the last decade due to their stable and non-toxic characteristics [11, 12] and have been widely used for the electrodeposition of several metals [13–16]. We preferred DES over aqueous electrolyte due to better film-forming characteristics of the former.

2 Experimental

2.1 Materials

Zinc (II) chloride ($ZnCl_2$, Merck, 98%), Zinc (II) sulfate (Sıgma-Aldrich, 99%), Nickel (II) chloride hexahydrate ($NiCl_2.6H_2O$, Merck, 98%), Choline chloride ($HOC_2H_4N(CH_3)_3Cl$, Merck, 98%), Ethylene glycol (EG) (Sıgma-Aldrich, 99%), Potassium hydroxide (KOH, Merck, 90%) were used as purchased.

2.2 Electrode preparation

Electrolyte solutions for the electrodeposition of Ni-only and Ni-Zn coatings were prepared by dissolving a total amount of 5 mmol $NiCl_2$-$6H_2O$ and $ZnCl_2$ salts in 10 mL of 1:2 molar ratio choline chloride-ethylene glycol deep eutectic solvent (DES) at 60 °C. For Ni-Zn binary coatings, $NiCl_2$-$6H_2O$ to $ZnCl_2$ mole ratio in DES was selected as 4:1, 2:1, 1:1 and 1:2. From now on, the electrodes made from these electrolytes will be denoted as NiZn 41, NiZn 21, NiZn 11 and NiZn 12, respectively. The coatings were deposited onto 1 cm^2 copper foils that were polished prior to deposition. The back side of the foil was insulated using a tape before immersing into DES. Pt and Ag/AgCl electrodes were used as counter and reference electrodes in all depositions, respectively. Ni-only coatings were deposited at 5 different cathodic potentials, namely − 1.3 V, − 1.2 V, − 1.1 V, − 1.0 V and − 0.8 V vs. Ag/AgCl. Ni-Zn coatings were obtained at -1.0 V vs. Ag/AgCl. The electrodeposition processes were stopped for all samples when a total charge of 3 As cm^{-2} was passed. For the anodic dealloying of zinc from coatings, electrodeposited electrodes were immersed into 0.5 M aqueous $ZnSO_4$ solution together with a Zn plate (used as both counter and reference electrode) and current was allowed to pass until potential stabilized around 1.0 V vs. Zn/Zn^{+2}.

2.3 Supercapacitor testing

Ni-only and Ni-Zn thin films were dipped into 0.1 M KOH solution and charged to 1.2 V vs. Ag/AgCl twice in order to activate the electrodes. Later, cyclic voltammetry scans were taken at 10 mV s^{-1} scan rate between 0–0.7 V to determine capacitive characteristics. For more detailed analysis, NiZn 11 electrode was selected and its galvanostatic and cyclic voltammetry tests were conducted at 5 A g^{-1}, 10 A g^{-1}, 20 A g^{-1} and 2 mV s^{-1}, 5 mV s^{-1}, 10 mV s^{-1} and 20 mV s^{-1} rates, respectively.

2.3.1 Physical analysis

Crystal structure analysis of thin films was performed using PANalytical Empyrean X-ray diffractometer using CuKα radiation. The diffraction patterns were collected between $2\theta = 30°$ and 80° at a scan rate of 2° min^{-1}. The surface roughness analyses of films were carried out using Quanta 650 Field Emission Scanning Electron Microscope

and Park NX10 Atomic Force Microscope. For elemental analysis, EDS unit attached to SEM was used.

3 Results and discussion

Ni-only electrodes were electrodeposited at five different potentials and the variation of deposition currents with time are given in Fig. 1 for all samples. Integrated areas in all samples correspond to 3 As cm^{-2}. The cathodic currents rise with deposition potentials as higher potentials create a larger driving force for ion transport in the electrolyte. Once a minimum cathodic current is reached shortly after the start of electrodeposition, it rises again. The pace of rise in current is faster in particular for − 1.1, − 1.2 and − 1.3 V samples. These reversal points are marked with black arrows on the figure. It was noticed during deposition that bubble release accelerated after this point, which is attributed to the generation of hydrogen gas caused by the electroreduction of deep eutectic solvent. As the deposition potential gets more cathodic, DES becomes less stable electrochemically and more hydrogen gas is generated. Besides this, the arrows are seen to shift to shorter durations with increasing deposition potentials. This is explained by the fact that nickel surface is more catalytic than copper surface in terms of electroreduction of the solvent. In other words, the faster the copper foil is covered with nickel coating, the quicker the start of gas formation.

The cyclic voltammetry (CV) scans of Ni-only electrodes for the first five cycles are given in Fig. 2. The cathodic peak current of electrode deposited at -0.8 V is only 1 mA cm^{-2}. It quickly rises to 17 mA cm^{-2} with -1.0 V sample and tops at 43 mA cm^{-2} with − 1.1 V electrode. Besides these results, it is noticed as a general trend that the separation between

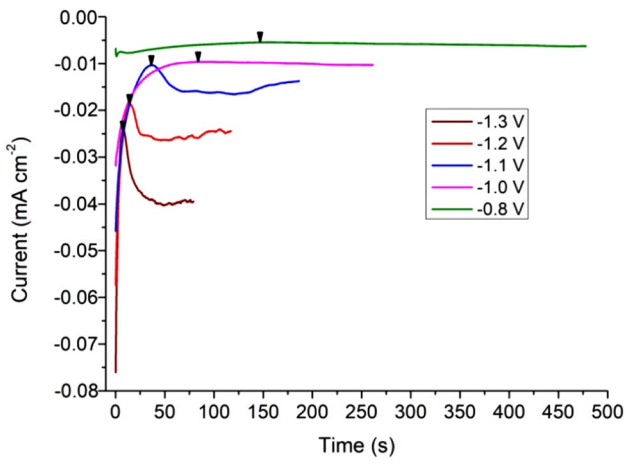

Fig. 1 The variation of deposition currents with time for Ni-only electrodes electrodeposited at different potentials (vs. Ag/AgCl reference electrode)

anodic and cathodic peaks, in other words polarization, gets wider with increasing peak current. Specifically, it ranges from 80 mV for − 0.8 V to 410 mV for − 1.2 V electrodes.

In order to explain the difference in the electrochemical activity of different electrodes, surface morphology of films was examined using Scanning Electron Microscope. The photos of films deposited at − 1.3 V and − 0.8 V are given in Fig. 3a-b. The difference in the surface texturing of films deposited at the most cathodic and the least cathodic potentials is easy to distinguish. While -0.8 V electrode has the appearance of a smooth surface with full coverage, − 1.3 V electrode consists of a cracked film at the bottom and half spherical shapes at the top. This morphology is due to the release of extensive amount of hydrogen bubbles during deposition, causing stress on thin film. Such a texture results in enlarged surface area of nickel film, thereby explaining much higher capacitance values for − 1.1, − 1.2 and − 1.3 V electrodes. On the other hand, − 0.8 V electrode ends up with a smaller surface area and poorer supercapacitor activity.

Linear sweep voltammetry profiles of electrolytes containing $NiCl_2$-only as well as various ratios of $NiCl_2$ to $ZnCl_2$ salts are shown in Fig. 4. Two cathodic peaks can be noted on the profiles. The first peak around -450 mV vs. Ag/AgCl is due to the reduction of Ni^{+2} ions to metallic Ni^0. The second peak is around -1020 mV and corresponds to the reduction of Zn^{+2} to Zn^0. This peak is absent in $NiCl_2$-only electrolyte as expected. In order to isolate the impact of zinc dealloying on surface morphology, the electrodeposition of Ni-Zn coatings was executed at -1.0 V where hydrogen bubble formation was minor and zinc deposition still occurred. In order to ascertain Ni and Zn mole ratios in the films, energy-dispersive spectroscopy (EDS) analyses were done. The mole percentage of nickel was found to be 93%, 91%, 89% and 86% in NiZn 41, NiZn 21, NiZn 11 and NiZn 12 coatings, respectively. In Ni-Zn binary phase diagram, zinc can be seen to dissolve up to 20 mol % in nickel, thereby forming a solid solution. Based on EDS numbers, a single nickel phase can be expected. Indeed, X-ray diffraction profiles of four coatings in Fig. 5 reveal a single nickel phase whose intensity diminishes with increasing $ZnCl_2$ amount in the electrolyte [17–20]. These results suggest that insertion of zinc into nickel had amorphization effect.

The zinc element was removed from Ni-Zn films via anodic dealloying using aqueous $ZnSO_4$ solution. The zinc plate was used as both counter and reference electrodes. The change of potential with time in NiZn 12 electrode is given as an example in Fig. 6. The potential starts around 0.5 V vs. Zn/Zn^{+2}, rises almost vertically to 1.05 V vs. Zn/Zn^{+2} and stabilizes afterward at this potential. The dealloying process was stopped right after the flattening of voltage curve as pointed out by black arrow in the figure. It must be pointed out that zinc removal occurs via a vertical rise in

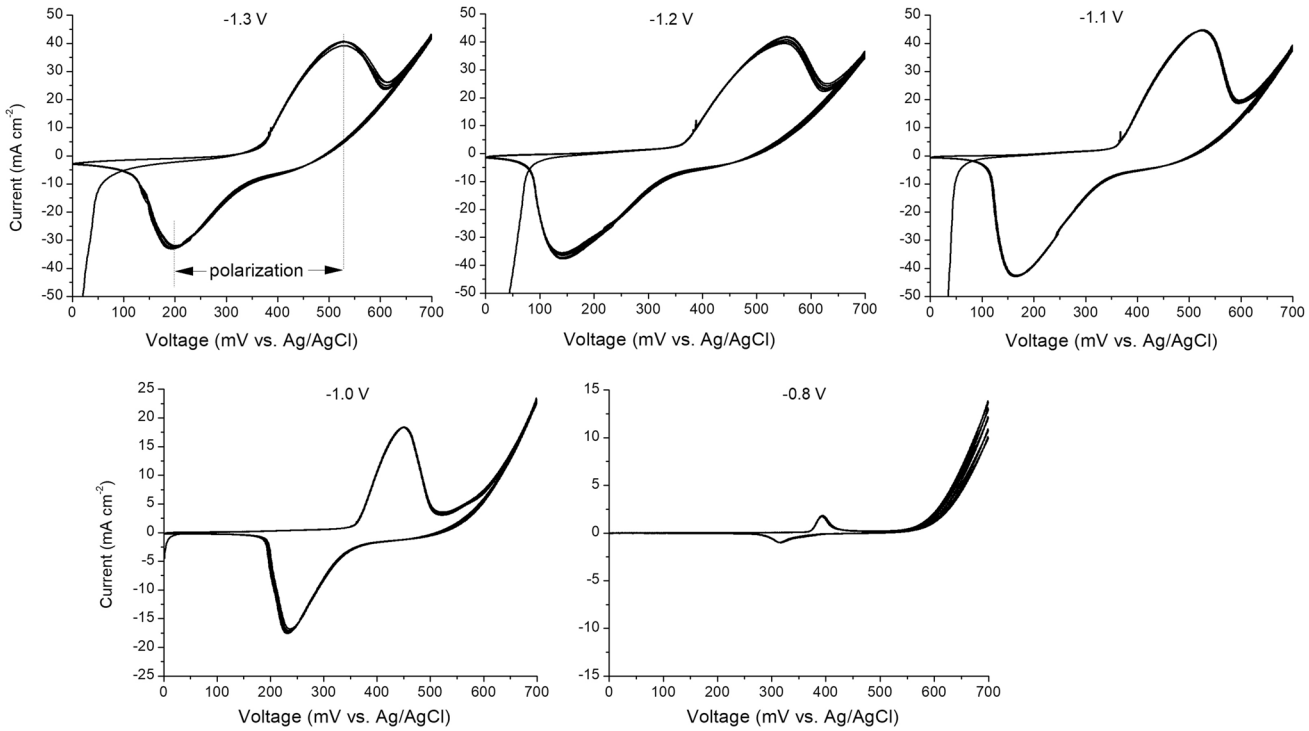

Fig. 2 Cyclic voltammetry scans of Ni-only electrodes in the first 5 cycles

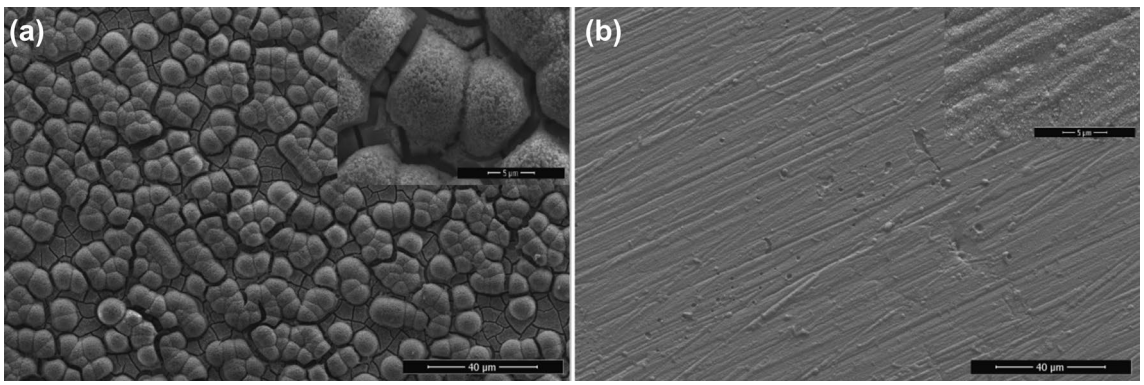

Fig. 3 SEM photos of Ni-only coatings electrodeposited **a** at − 1.3 V vs. Ag/AgCl **b** at − 0.8 V

potential rather than along a flat pleateau. This is probably because zinc extraction from nickel-zinc solid solution gets thermodynamically more challenging and energy consuming as zinc concentration gets more scarce. It must be pointed out that some nickel element might pass into the solution during dealloying step together with zinc.

The CV scans of four binary electrodes after zinc dealloying step are shown in Fig. 7a-d. The peak cathodic currents are 17, 21, 24 and 31 mA cm^{-2} for NiZn 41, NiZn 21, NiZn 11 and NiZn 12 samples, respectively. The results indicate that capacitance of electrodes increases with $ZnCl_2$ concentration in the deep eutectic solvent. As EDS results proved that the amount of zinc deposited gets larger with increasing zinc ion concentration in the electrolyte, their removal during anodic dealloying results in larger supercapacitor activity. As with the case of Ni-only electrodes, SEM photos of NiZn 12 coatings before and after dealloying step were taken and illustrated in Fig. 8a-b. It is clearly seen that the smooth surface prior the dealloying takes a rougher form with hills and pits in nanoscale following zinc extraction. In order to corroborate electron microscopy results, Atomic Force Microscope (AFM) was used to picture the surface of dealloyed NiZn 41, NiZn 21, NiZn 11 and NiZn 12 samples covering an area of 25 × 25 µm (Fig. 9a-d). The average

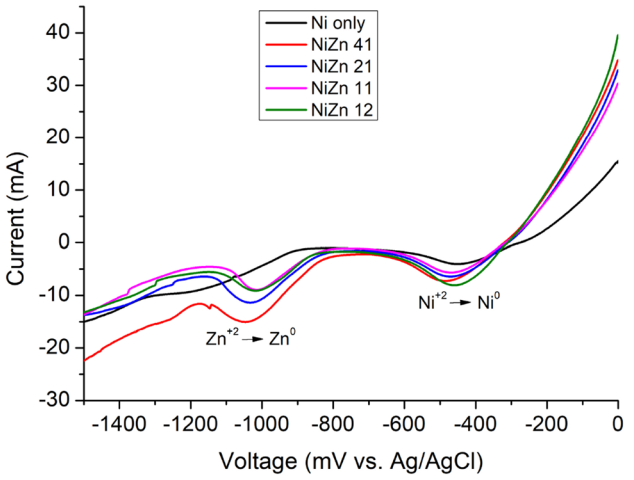

Fig. 4 Linear sweep voltammetry curves of deep eutectic solvents with different ratios of $NiCl_2$ and $ZnCl_2$ salts

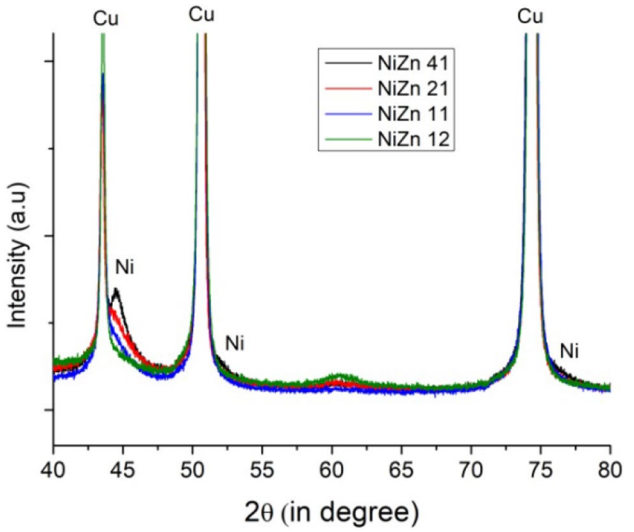

Fig. 5 X-ray diffraction patterns of Ni–Zn coatings deposited from electrolytes with different ratios of $NiCl_2$ and $ZnCl_2$ salts

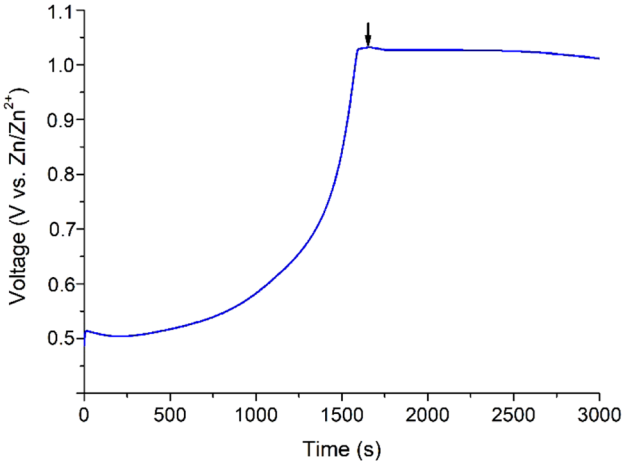

Fig. 6 Variation of potential with time during zinc dealloying process

roughness (R_a) of electrode surface increases consistently with the amount of zinc dealloyed from binary electrodes. In order to emphasize the role of dealloying process in R_a, AFM photo of NiZn 12 sample prior to zinc removal was also taken and displayed in Fig. 9e. The R_a number is only 19 nm and is significantly lower than its dealloyed counterpart. Based on SEM and AFM results, it is concluded that besides hydrogen bubble generation during electrodeposition, the dealloying process can be used to create a rough surface texture with increased total surface area. This is interpreted as the basis of enhanced capacitance in studied electrodes. In order to further substantiate the claim that surface roughening is critical for supercapacitor activity, sister electrodes of all four Ni-Zn coatings were prepared and electrochemically evaluated with their as-deposited forms (i.e., no dealloying). The results are summarized in Fig. 7e. The peak currents of electrodes with no dealloying lie in the range of 2–5 mA cm^{-2} and are significantly smaller than those of dealloyed electrodes. It is revealed unequivocally that dealloying step is crucial to achieve high capacitance numbers. The anodic current was passed for a certain duration of time on Ni-only electrode to accentuate the role of zinc removal in dealloying process. For this experiment, Ni electrode deposited at -0.8 V was selected as it had the smoothest surface and the smallest capacitance values. Upon the passage of anodic current (i.e., some nickel was dissolved from the coating), the peak current of this electrode jumped from 1 to 4.8 mA cm^{-2}. The increase is much smaller than those seen with binary electrodes, thereby demonstrating that zinc dissolution induces a rougher surface than nickel dissolution and is the major reason behind capacitance rise. As a final note, zinc-only film coated onto copper substrate yielded no supercapacitor acitivty, proving that nickel is the only element contributing to capacitive behavior.

It was mentioned previously in the text that a correlation between peak cathodic current and polarization was noticed during cyclic voltammetry analyses. These values were gathered for all CV measurements performed in this study and plotted in Fig. 10a. A linear relationship is clearly visible between these two parameters, namely electrodes with more capacitance exhibit more polarization. We are not aware of a study that has reported this correlation before. The mechanism of capacitance in nickel-based electrodes is based on following redox reaction; $Ni(OH)_2 + OH^- = NiOOH + H_2O + e^-$ [21, 22]. The X-ray diffraction results showed that coatings contain metallic nickel phase only. This metallic phase

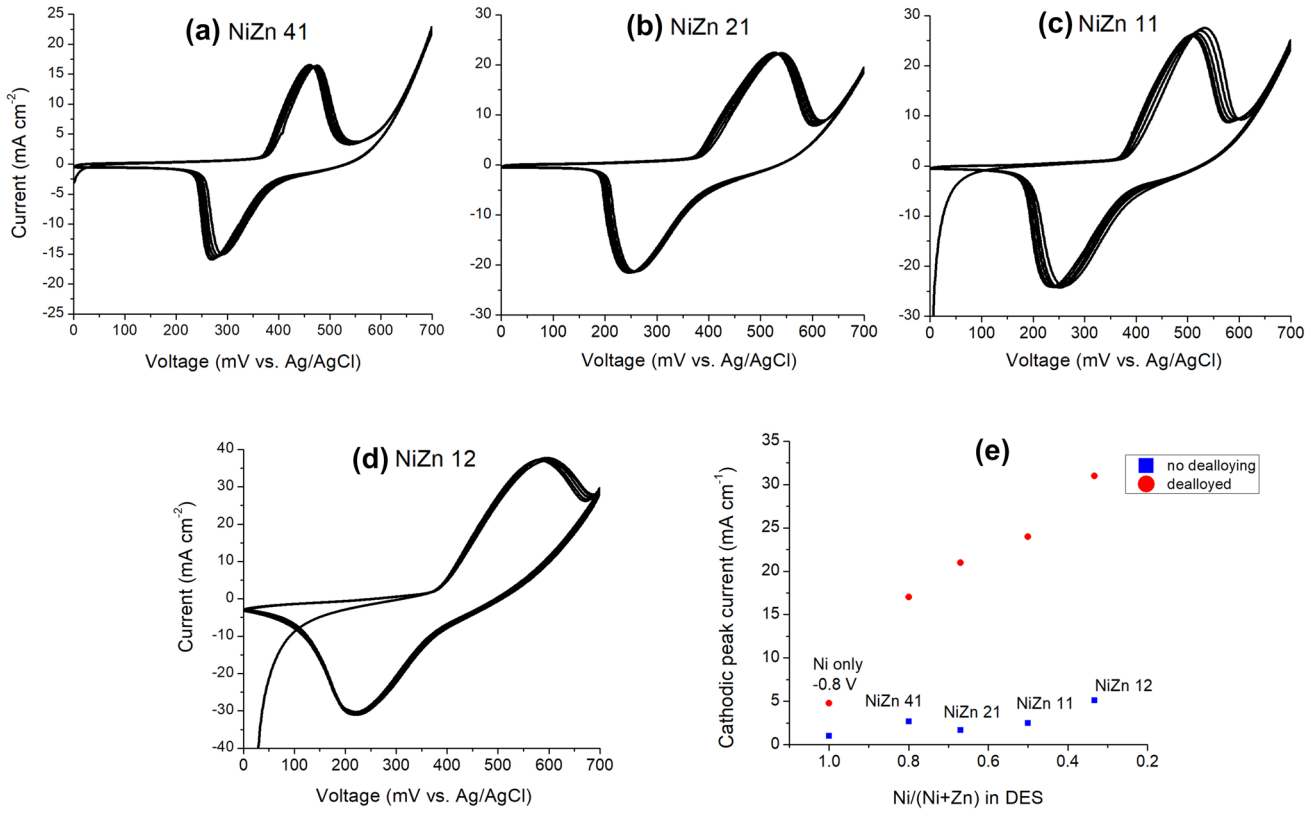

Fig. 7 **a**–**d** Cyclic voltammetry scans of Ni–Zn electrodes in the first 5 cycles **e** comparison of cathodic peak currents for different 'dealloyed' and 'non-dealloyed' electrodes

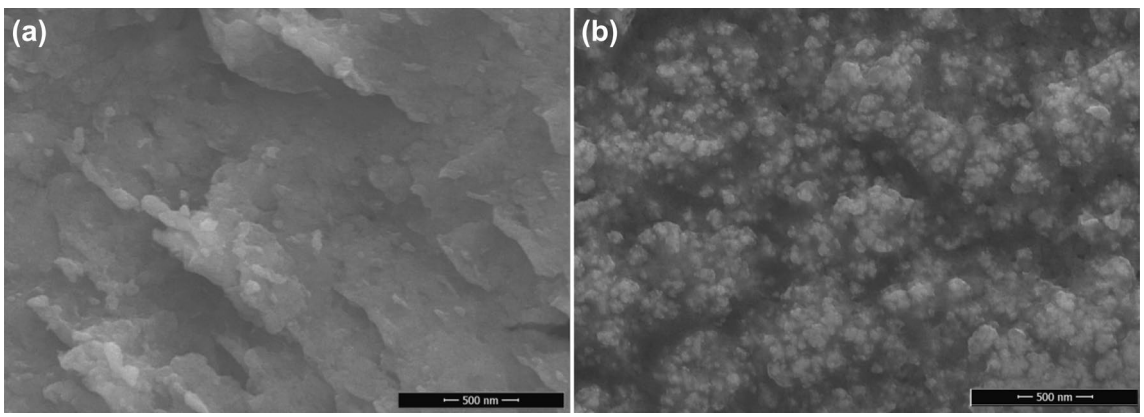

Fig. 8 SEM photos of NiZn 12 coating **a** before dealloying **b** after dealloying

needs to convert into nickel hydroxide to induce electrochemical activity. Therefore, it can be reasoned that whichever electrode exhibits more capacitance, more of this metallic nickel phase must have converted during electrochemical tests. Knowing that nickel hydroxide is a poor electrical conductor, it can be argued films with high capacitance should suffer from low electrical conductivity, thereby resulting in high polarization. In order to test this hypothesis, X-ray diffraction patterns of Ni-only electrodes were compared before and after supercapacitor measurements. In Fig. 10b, the intensity of nickel peaks is seen to shrink following electrochemical testing

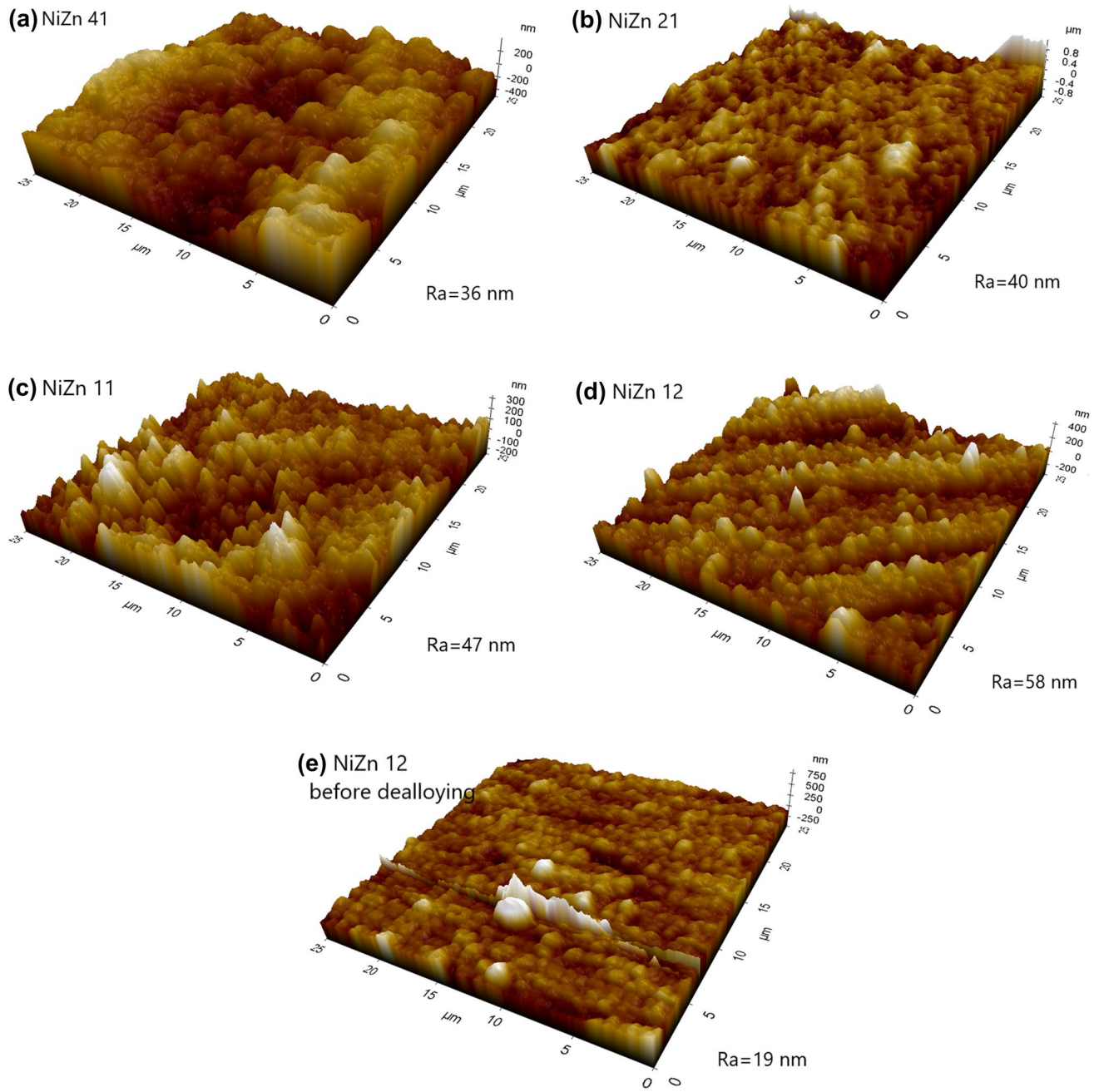

Fig. 9 AFM photos of electrodes **a** dealloyed NiZn 41 **b** dealloyed NiZn 21 **c** dealloyed NiZn 11 **d** dealloyed NiZn 12 **e** NiZn 41 before dealloying

as demonstrated with − 1.0 V Ni coating, consistent with our hypothesis. Another observation is that the intensities of the same nickel peaks get smaller with higher deposition potentials. Given that − 1.2 V and − 1.3 V electrodes have higher peak currents than − 1.0 V electrode, this observation agrees well with the above hypothesis. It is more difficult to observe the above-mentioned phenomena in electrodes containing a carbon-based material to help electronic conductivity. This is because of the fact that even though electroactive material's conductivity degrades during electrochemical cycling, the carbon-based material still endures and minimizes its impact on electrode polarization. As a final note, no crystalline nickel hydroxide peaks are visible in X-ray data in electrochemically tested electrodes, suggesting amorphous nature of this phase.

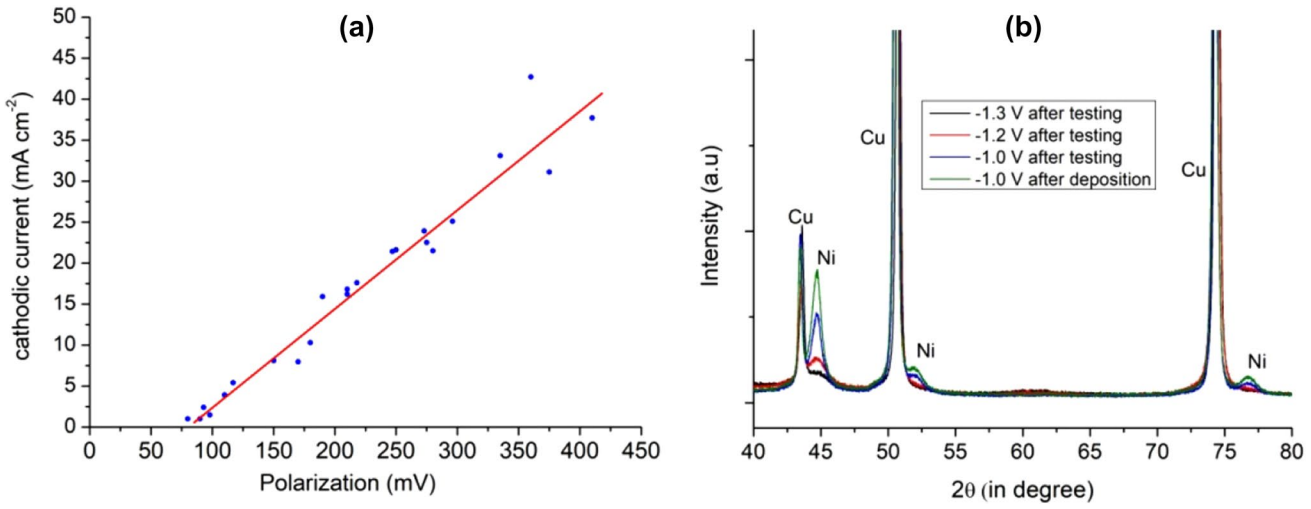

Fig. 10 **a** Plot of cathodic peak current vs. polarization values extracted from overall 23 cyclic voltammetry measurements **b** X-ray diffraction patterns of Ni-only electrodes deposited at different potentials

For more detailed supercapacitor tests, NiZn 11 electrode was chosen and galvanostatic and cyclic voltammetric cycles at varying rates were undertaken. In order to determine the mass of deposit on copper foil, Faraday's electrolysis law was used;

$$F = \left(I \cdot t \cdot M_w\right)/(z \cdot 96485) \quad (1)$$

where I is the current in Amper, t is time in seconds, M_w is the molar mass of NiZn coating, z is the oxidation state of metallic ions and 96,485 is Faraday's constant. It was 3 As in all of our experiments, M_w was calculated to be 59.5 g mol^{-1} based on 89–11% mole ratio of Ni and Zn elements and finally z = 2. Based on these values, the mass of coating was calculated to be 0.925 mg assuming 100% electrolysis efficiency. This mass was used in galvanostatic current and capacitance calculations.

The galvanostatic voltage curves of NiZn 11 electrode at 5 A g^{-1}, 10 A g^{-1} and 20 A g^{-1} current densities are given in Fig. 11a. The electrode reaches a specific capaticance of 685 F g^{-1} at 5 A g^{-1}. Such a high number is comparable to its equivalents in literature [23–26]. Figure 11b shows the CV curves of NiZn 11 in 0.5 M KOH electrolyte at scan rate of 2, 5, 10 and 20 mV s^{-1}. The potentials of oxidation/reduction peaks shifts to more positive/negative values with increasing scan rate due to polarization effect and the internal resistance of electrode. The relationship of $i = c\nu b$ was reported previously to evaluate charge-storage kinetics, where i and ν refer to the peak current of CV curves and scan rate, respectively and c is a constant [17, 27, 28]. In these studies, battery-like behavior was identified for b = 0.5 and capacitive behavior for b = 1. Figure 10c presents the log(i) versus log(ν) plots for both cathodic and anodic scans. The b values of 0.60 and 0.61 were calculated for our electrode indicating that the battery-type behavior dominated the charge storage.

4 Summary

Ni-only and Ni-Zn binary thin films were electrodeposited onto copper substrates using choline chloride-ethylene glycol deep eutectic solvent and evaluated as supercapacitor electrodes. The surfaces of electrodes were strategically roughened to increase the overall surface area and with that electrochemical activity. In order to reach this goal, two very different methods were adopted. They included generating hdyrogen gas during electrodeposition by lowering deposition potential and dealloying of zinc atoms from electrodes in a post-deposition step. Both methods were found to significantly enhance the specific capacitance of electrodes. A linear relationship was established between the cathodic peak currents and the polarization numbers extracted from the cyclic voltammetry scans of several electrodes, possibly for the first time in literature here. The electrode polarization, i.e., the separation between peaks, got larger with rising peak current values. The underlying reason behind such phenomena was based on diminishing electronic conductivity of electrodes resulting from transformation of metallic nickel phase into nickel hydroxide upon electrochemical testing. In

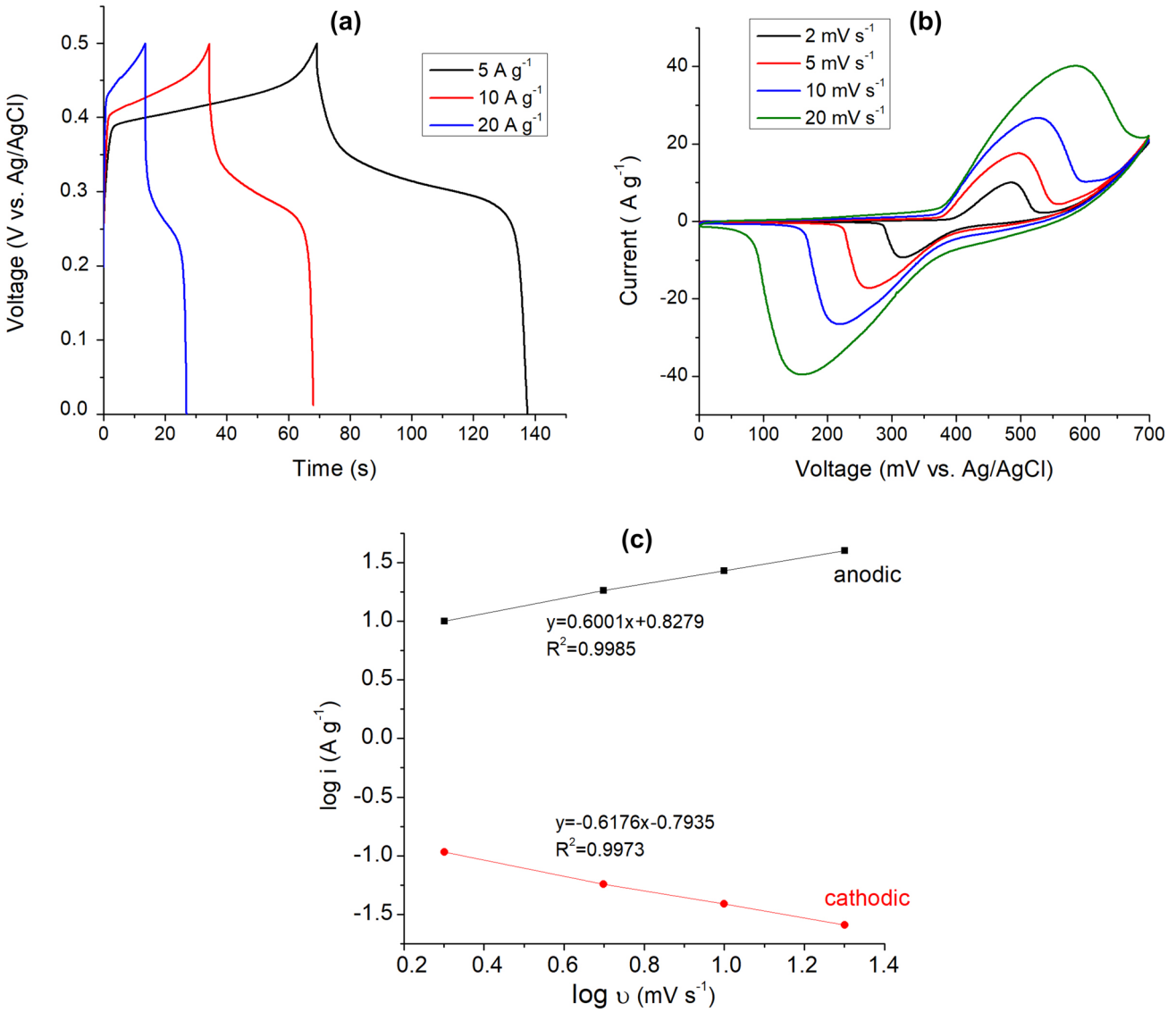

Fig. 11 **a** Galvanostatic voltage profiles **b** CV scans **c** log i vs. log ν plots of NiZn 11 electrode

our future studies, we will focus on this aspect and devise solutions to minimize polarizaton without compromising specific capacitance.

Supplementary Information The online version contains supplementary material available at https://doi.org/10.1007/s00339-021-04784-3.

References

1. G. Cai, X. Wang, M. Cui, P. Darmawan, J. Wang, A. Lee-Sie, P. See Lee, Nano Energy 12, 258 (2015)
2. Y. Zhang, H. Feng, X. Wu, L. Wang, A. Zhang, T. Xia, H. Dong, X. Li, L. Zhang, Int. J. Hydrog. Energy **34**, 4889 (2009)
3. M. R. Manikandan, K. P. Cai, Y. D. Hu, C. L. Li, J. T. Zhang, Y. P. Zheng, Y. F. Liang, H. R. Song, M. Y. Shang, X. N. Shi, . X. Zhang, S. Q. Yin, S. Y. Shang, X. W. Wang, Appl. Phys. A, 127, (2021).
4. S. Verma, A. Khosla, S. Arya, J. Electrochem, J. Electrochem. Soc. **167**, 120527 (2020)
5. G.C. Zhang, J. Zhong, M. Xu, Y. Yang, Y. Li, Z. Fang, S. Tang, D. Yuan, B. Wen, J. Gu, Chem. Eng. J. **375**, 122093 (2019)
6. G. Cheng, Y. Yan, R. Chen, New J. Chem. **39**, 676 (2015)
7. A.P. Abbott, A. Ballantyne, R.C. Harris, J.A. Juma, K.S. Ryder, G. Forrest, Electrochim. Acta **176**, 718 (2015)
8. Z. Wu, L. Liu, B. Shen, C. Zhong, W. Hu, Mater. Sci. Eng.A 556**,** 767 (2012).
9. A.P. Abbott, D. Boothby, G. Capper, D.L. Davies, R.K. Rasheed, J. Am. Chem. Soc. **126**, 9142 (2004)
10. Y. Dai, J. van Spronsen, G.J. Witkamp, R. Verpoorte, Y.H. Choi, Anal. Chim. Acta. **766**, 61 (2013)
11. E. Shabani, D. Zappi, L. Berisha, D. Dini, C. Sadun, Talanta **215**, 120880 (2020)

12. S. Karimi, H. Shekaari, I. Ahadzadeh, J. Taiwan Inst. Chem. Eng. **117**, 1 (2020)
13. C. Andrew, M.O. Aremu, O.A. Ushie, FUW Trends Sci. Technol. **1**, 321 (2016)
14. A. Florea, L. Anicai, S. Costovici, F. Golgovici, T. Visan, Surf. Interface Anal. **42**, 1271 (2010)
15. H.F. Alesary, S. Cihangir, A.D. Ballantyne, R.C. Harris, D.P. Weston, A.P. Abbott, K.S. Ryder, Electrochim. Acta **304**, 118 (2019)
16. M.A. Miller, J.S. Wainright, R.F. Savinell, J. Electrochem. Soc. **164**, A796 (2017)
17. Z. Dai, L. Xue, Z. Zhang, Y. Gao, J. Wang, Q. Gao, D. Chen, Energy Fuels **34**, 10178 (2020)
18. I. El-Hallag, S. Elsharkawy, S. Hammad, Int. J. Hydrogen Energy **46**, 15442 (2021)
19. M.Y. Rafique, L. Pan, W.S. Khan, M.Z. Iqbal, H. Qiu, M.H. Farooq, M. Ellahi, Z. Guo, CrystEngComm **15**, 5314 (2013)
20. X.W. Wei, X.M. Zhou, K.L. Wu, Y. Chen, CrystEngComm **13**, 1328 (2011)
21. K. Song, W. Li, R. Yang, Y. Zheng, X. Chen, X. Wang, G. Chen, W. Lv, Electrochim. Acta Available online 21 May 2021, 138663
22. A. Yavuz, N. Ozdemir, P.Y. Erdogan, H. Zengin, G. Zengin, M. Bedir, Appl. Phys. A **125**, 494 (2019)
23. S. Chen, G. Yang, H. Zheng, Electrochim. Acta **220**, 296 (2016)
24. L. Li, R. Li, S. Gai, F. He, P. Yang, J. Mater. Chem. A **2**, 8758 (2014)
25. H. Wan, L. Lv, L. Peng, Y. Ruan, J. Liu, X. Ji, L. Miao, J. Jiang, J. Power Sources **286**, 66 (2015)
26. Q. Zhang, B. Zhao, J. Wang, C. Qu, H. Sun, K. Zhang, M. Liu, Nano Energy **28**, 475 (2016)
27. H.-S. Kim, J.B. Cook, H. Lin, J.S. Ko, S.H. Tolbert, V. Ozolins, B. Dunn, Nat. Mater. **16**, 454 (2017)
28. J. Wang, J. Polleux, J. Lim, B. Dunn, J. Phys. Chem. C **111**, 14925 (2007)

Authors and Affiliations

Muharrem Kunduraci[1] · Doğan Çirmi[2] · Selda Doğan Çalhan[3] · Uğur Çağlayan[4]

[1] Department of Aerospace Engineering, Tarsus University, Mersin, Turkey

[2] Department of Chemistry, Mersin University, Mersin, Turkey

[3] Department of Pharmaceutical Biotechnology, Mersin University, Mersin, Turkey

[4] Central Research Laboratory, Cukurova University, Adana, Turkey